# Statistically Significant of Time-varying Neural Connectivity using Generalized Partial Directed Coherence

Pedro L. C. Rodrigues and Luiz A. Baccalá

***Abstract*— This paper illustrates the effectiveness of generalized partial directed coherence (gPDC) in characterizing time-varying neural connectivity by properly generalizing its single trial asymptotic statistical results to a multi trial setting under a time sliding-window procedure is. Toy model simulations and real EEG data are used for benchmarking purposes.**

## I. INTRODUCTION

The focus of neural connectivity studies is starting to shift from determining the brain's quiescent link structure towards describing how its connectivity evolves during cognitive tasks [1], [2], [3]. These works share a means of estimating connectivity allied to quantifier time tracking procedures. For example, in the EEG processing context, Granger causality estimators have become popular in association with time-varying features that are usually tracked via alternative approaches: either through sliding-window [4] estimation or via recursive least-squares (RLS) algorithm [5].

Here, we stress the sliding-window time-varying approach to generalized partial directed coherence ($g$PDC) [6] presented in [7] by modifying $g$PDC's single trial asymptotic statistical significance criteria from [8] to a multi trial setting. In addition to showing the plausibibility of the corrected criteria, we further show its usefulness when describing a system comprising a pair of interacting neural mass models. Finally, to further illustrate the practical usefulness of the approach, we apply it to a publicly available dataset, and contrast it to the results in [3] that employ the same data.

After a brief presentation of the technical details of our estimation procedure (Sec. II-A), we overview how to assess its statistical significance (Sec. II-B) that are next applied to simulated EEG signals followed by consideration of a real dataset (Sec. III). After a brief discussion (Sec. IV), we finish with some final comments (Sec. V).

## II. MATERIAL AND METHODS

After a brief recap of $g$PDC, we follow with a description of the adopted statistical testing methodology. Next, we examine the neural mass model used for numerical performance illustration. Finally, we provide additional details about the real EEG dataset.

The authors are with the Telecommunications and Control Department of Escola Politécnica, University of São Paulo, São Paulo, Brazil, 05508-900 prodrigues@usp.br baccala@lcs.poli.usp.br

### A. Time-varying connectivity estimation

Simultaneous recordings from $m$ channels (viz. electrodes) are represented by a multivariate time series

$$\mathbf{x}(n) = \begin{bmatrix} x_1(n) \\ \vdots \\ x_m(n) \end{bmatrix}.$$

A multivariate autoregressive model (MVAR) for this process is

$$\mathbf{x}(n) = \sum_{l=1}^{p} \mathbf{A}(l)\mathbf{x}(n-l) + \mathbf{w}(n), \qquad (1)$$

where $p$ is the model order, $\mathbf{w}(n)$ stands for a zero mean Gaussian stationary innovation process with covariance matrix $\mathbf{\Sigma_w}$, and the $\mathbf{A}(\cdot)$ coefficients are $m \times m$ matrices.

Adequate fitting of (1) usually calls for sufficiently long quasi-stationary time series to be available. When this usual premise is not met, it is, however, possible to by-pass this demand, and study time-varying connectivity studies if multiple data evolution trials that describe the same phenomenon are available. The underlying presumption is that, collectively, the $N_t$ trial series represent the evolution of the same system so as to allow the construction of a single joint representative summary model (see [7] for more details).

Causal relations between channels $i$ and $j$ can then be described in the frequency domain via gPDC:

$${}_g\pi_{ij}(f) = \frac{\frac{1}{\sigma_{ii}}\bar{A}_{ij}(f)}{\sqrt{\sum_{k=1}^{m}\frac{1}{\sigma_{kk}^2}|\bar{A}_{kj}(f)|^2}} = \frac{\frac{1}{\sigma_{ii}}\bar{A}_{ij}(f)}{{}_g\pi_d(f)}, \qquad (2)$$

where $\sigma_{ii}^2$ is the $i$th element in $\mathbf{\Sigma_w}$'s main diagonal,

$$\bar{A}_{ij}(f) = \begin{cases} 1 - \sum_{l=1}^{p} a_{ij}(l)e^{-\mathbf{j}2\pi f l}, \text{ if } i = j \\ -\sum_{l=1}^{p} a_{ij}(l)e^{-\mathbf{j}2\pi f l}, \text{ otherwise} \end{cases}, \qquad (3)$$

with $\mathbf{j} = \sqrt{-1}$, and $a_{ij}(l)$ corresponds to position $(i,j)$ of matrix $\mathbf{A}(l)$ in Equation 1. Nullity of ${}_g\pi_{ij}(f)$ indicates absence of Granger causality from time series $x_j(n)$ to $x_i(n)$ at the normalized frequency $f$.

To gauge $g$PDC's temporal dynamics, we employ a rectangular $L$ point long sliding window to estimate a MVAR model associated to each time instant $n$, i.e. each joint model refers to the $(n-L+1, n)$ time interval. Let ${}_g\pi_{ij}(f,n)$ denote the corresponding $g$PDC time-frequency representation.

In the examples that follow, a single model order $p$ was selected for all windows using Akaike's Information Criterion [9] based on the examination of its maximum value in a random subset of record windows.

### *B. Extension of gPDC's statistical theory to the short segment case*

Under the null hypothesis $\mathcal{H}_0 :_g \pi_{ij}(f) = 0$, one can show [8] that

$$n_s \; {}_g\pi_d(f) \; (|\widehat{{}_g\pi}_{ij}(f)|^2 - |{}_g\pi_{ij}(f)|^2) \xrightarrow{d} \sum_{k=1}^{q} l_k(f)\chi_1^2 \quad (4)$$

holds asymptotically for $n_s \to +\infty$, wherefrom proper decision thresholds can be computed at the desired level of $\alpha$ significance. To use (4) in the context of short segments, one must replace $n_s$ by an appropriate quantity. Through extensive simulations, our empirical investigation has shown that the desired Type I error rate can be attained by taking $n_s = N_t \times (L-p)$. A similar $n_s$ equivalent value substitution holds when determining confidence intervals if $\mathcal{H}_0$ can be rejected [8]. To provide the reader with some sense of the effectiveness of this correction under the best possible circumstances, we emulate [10] by simulating the system in Figure 1 and gauging its $g$PDC performance as function of the strength of the $1 \to 2$ connection.

### *C. Neural mass models*

First proposed as means for studying EEG alpha-rhythym generation in the thalamus [11], neural mass models consists of non-linear equations that are physiologically inspired by the interaction between pyramidal cells and interneurons (excitatory and inhibitory) over cortical columns.

In our simulations, we employed an adapted version of [11]'s proposal that models the connection between different cortical columns together with the generation of evoked potentials [12]. We specifically implemented [13]'s suggestions as to how to model for cortical columns that oscillate at frequencies other than the alpha band.

### *D. Real EEG data*

To provide a practical real context where this approach might be profitably used, we selected the publicly available EEG recordings[1] collected, analyzed, and described by [14] whose dataset consists of multichannel recordings obtained during whisker stimulation of p21 Wistar rats at a sampling frequency of 2kHz, and consisting of 50 trials for each rat and each type of stimulus (right or left whisker). Figure 6(A) sums up rat electrode scalp positions.

Under this protocol, whisker stimulus leads to a somatosensory evoked potential (SEP) on the rat's contralateral primary sensory cortex (cS1) after 5ms, with its activity lasting for approximately 20ms and later spreading to other cortical areas [14].

[1] `http://www.fbmlab.com/data/`

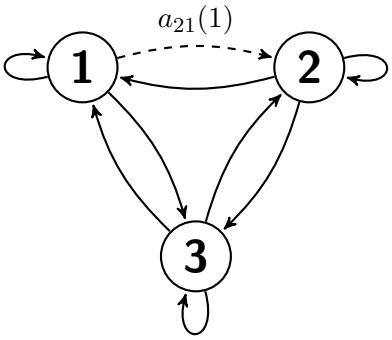


Fig. 1: Diagram depicting the network structure corresponding to the multivariate autoregressive model given by:

$$\begin{cases} x_1(n) = 0.2x_1(n-1) - 0.4x_2(n-1) \\ \qquad -0.2x_2(n-2) + 0.3x_3(n-1) + w_1(n) \\ x_2(n) = \boldsymbol{a_{21}}(1)x_1(n-1) + 0.8x_2(n-1) \\ \qquad -0.1x_2(n-2) + 0.4x_3(n-1) + w_2(n) \\ x_3(n) = 0.5x_1(n-2) - 0.1x_2(n-1) + 0.2x_2(n-2) \\ \qquad +0.4x_3(n-1) + 0.1x_3(n-2) + w_3(n) \end{cases}$$

where $\boldsymbol{a_{21}}(1) \in \{0, 0.05, 0.10, 0.15, 0.20, 0.50\}$.

| | | Percentage of rejection (%) | | | | | |
|---|---|---|---|---|---|---|---|
| | | $L = 12, N_t = 50$ | | $L = 12, N_t = 50$ | | $L = 600, N_t = 1$ | |
| $\boldsymbol{a_{21}}(1)$ | $\lvert{}_g\pi_{21}(0.3)\rvert^2$ | $\alpha = 5\%$ | $\alpha = 1\%$ | $\alpha = 5\%$ | $\alpha = 1\%$ | $\alpha = 5\%$ | $\alpha = 1\%$ |
| 0.00 | 0 | 8.56 | 2.91 | 5.86 | 1.63 | 5.19 | 1.06 |
| 0.05 | 0.0018 | 21.06 | 9.23 | 16.01 | 5.96 | 16.84 | 6.21 |
| 0.10 | 0.0070 | 56.15 | 35.17 | 47.90 | 26.05 | 53.98 | 30.03 |
| 0.15 | 0.0157 | 88.69 | 73.41 | 84.33 | 64.38 | 89.01 | 72.02 |
| 0.20 | 0.0275 | 99.03 | 95.66 | 98.16 | 92.07 | 99.23 | 95.82 |
| 0.50 | 0.1503 | 100.0 | 100.0 | 100.0 | 100.0 | 100.0 | 100.0 |
| | | Not corrected | | Corrected | | | |

TABLE I: Percentage (under 10000 Monte-Carlo trials) of $\mathcal{H}_0 : |{}_g\pi_{21}(f = 0.3)|^2 = 0$ with and without $n_s$ against the single-trial gold-standard case as a function of $a_{21}$.

## III. RESULTS

### *A. Empirical investigation*

Table I$\mathcal{H}_0$'s rejection rate as a function of $a_{21}$ with(Sec. II-B and without ($n_s = L \times N_T$) correction to an number of data points compared to a single-trial record of the same total number of points used as a gold standard.

### *B. Simulated NMM*

To further validate the present approach, we simulated EEG signals derived from a pair of interacting neural mass models (see Figure 2) whose link is suddenly severed and then switched back on again. Using a maximally overlapping sliding-window with $L = 30$ points and $p = 12$ leads to the estimated $g$PDC time-frequency evolution shown on Figure 5. A detailed comparative picture of $g$PDC between the "on" and the "off" state can be appreciated in Figure 3.

Connectivity evolution details at $41.18$ Hz are shown on Figure 5 for two window widths with their respective thresholds.

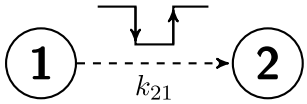


Fig. 2: Diagram of the connection between two neural mass models, oscilating respectively around the gamma (channel $1 \simeq 41$ Hz) and beta bands (channel $2 \simeq 22$ Hz) and directionally linked via $k_{21}$, which is turned off for 500 ms and then toggled back to its original value.

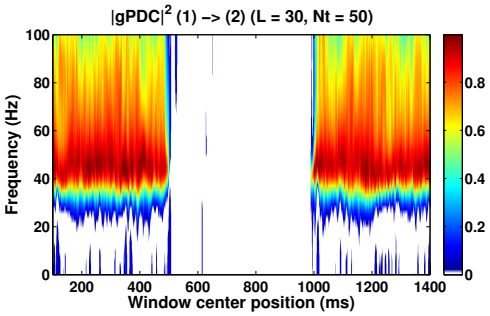


Fig. 3: The time-frequency representation of $|_g\pi_{21}|^2$ under the conditions of Figure 2 is shown against a white background that represents regions for which $\mathcal{H}_0$ cannot be rejected at $\alpha = 1\%$.

### C. Real EEG data

Figure 6 shows the results of processing real EEG neural activity from cS1 (electrode 4) for rat left whisker stimulation. To guarantee better estimates, only a subset of the 15 available channels (channels 2, 3, 4, 5, 6) was used, with a sliding window of $L = 30$ points and $p = 6$ chosen throughout the record.

## IV. DISCUSSION

These results show that our sliding-window algorithm manages to track connectivity changes in the context of both neural mass models and real EEG data.

Despite its practical importance, prior work on the statistics of time-varying connectivity estimators has resorted to resampling techniques [4] [15] [16], whose computer intensive nature do not take advantage of estimator's mathematical structure. Here we provide a computationally inexpensive tool for assessing the statistical significance of $_g\pi_{ij}(f, n)$'s estimates.

It is quite remarkable that, although the simulated EEG was generated with a non-linear set of equations, linear MVAR model estimation managed to capture the main signal interaction features that include the frequency activity peaks in each cortical column's spectrum (beta and gamma bands), and the direction of the connectivity between them. Furthermore, the thresholds of Figure 4(B) indicate that $_g\pi_{12}$'s peak during the ON state does not correspond to a causal influence from channel 2 toward channel 1.

One can readily notice the high variability of $g$PDC from $\text{NMM}_1$ to $\text{NMM}_2$ (Figure 5) which is nonetheless closely matched by decision thresholds and thereby allows correct inference within the prescribed confidence level.

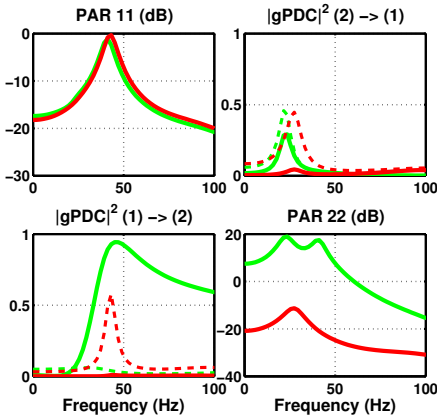


Fig. 4: Plot of $|_g\pi_{21}|^2$ and the estimated autospectrum of each channel when the connection between neural mass models is ON (**green**) and OFF (**red**). The dashed lines represent threshold values for the null hypothesis of no connection at a 1% significance value. Sampling frequency is 1000 Hz and the dataset has $N_t = 50$ realizations. Estimations were performed in windows of size $L = 30$.

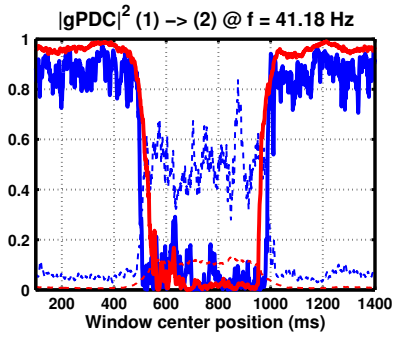


Fig. 5: Time evolution of $|_g\pi_{21}(f, n)|^2$ at frequency $f = 41.18$ Hz. The curve in **blue** portrays the results for estimations using $L = 30$ and in **red** for $L = 100$. Dashed lines represent null hypothesis rejection threshold values at $\alpha = 1\%$.

The analysis of the real EEG dataset was carried out so as to allow comparing results and methodology with those in [3]. Our sliding-window procedure differs from [3] who employ the RLS algorithm followed by averaging over trials. Whereas our connectivity inference employed just the $g$PDC between channels (with its immediate interpretation [17]), [3] opted for an alternative PDC version that is not only row-normalized, but which is also weighted by the values of a non-parametric estimate of each channel's power spectral density (PSD) [18] .

Despite differences in methodology, our results agree quite well with those in [3], even though we employ a somewhat simpler and well established neural connectivity estimator. Figures 6(B) and 6(C) show a peak in cS1's outward neural connectivity 10 ms after stimulus that fades out after approximately 25 ms, something that is compatible with what one would expect in this kind of experimental setup [14]. The present approach has the added advantage that it supplies a

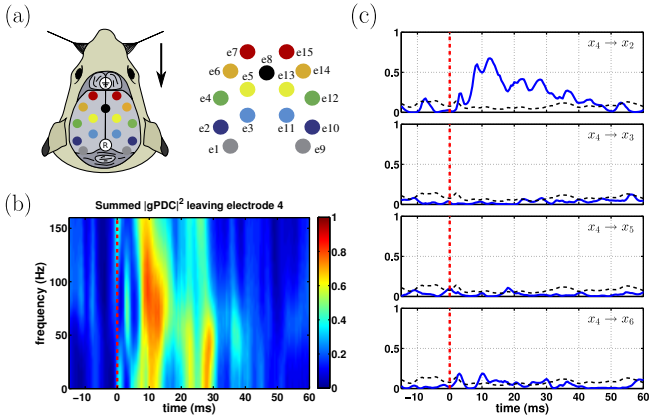


Fig. 6: Real EEG data estimation results using subject RN060616A [14]: (a) EEG electrode scalp positions. (b) Time-frequency representation of the summed $g$PDC leaving electrode 4 (cS1), i.e. $\sum_i |{}_g\pi_{i4}|^2$. (c) $g$PDC from electrode 4 towards electrodes 2, 3, 5 and 6 at frequency $f = 66.3$ Hz. Dashed **red** lines indicate the moment of whisker stimulus, whereas **black** ones represent threshold values at $\alpha = 5\%$.

well defined set of tools for the statistical characterization of the response.

One should note that [3]'s choice of connectivity estimator is heavily influenced by the characteristics of its MVAR model estimation method, which adopts a very small forgetting factor (equivalent to a large exponential sliding-window) which therefore leads to poor PDC time resolution in the time-frequency plane. The use of the non-parametric multiplicative PSD has the role of improving the time resolution even though it introduces a measure statistical uncertainty since its behaviour is not yet worked out. By contrast, the existing asymptotic statistics [8] for $g$PDC allowed introducing a method for ${}_g\pi_{ij}(f,n)$'s statistical significance assesment.

## V. FINAL COMMENTS

We proposed a new way for assessing the statistical significance of time-varying neural connectivity estimates, based on modifying existing asymptotic results.

Finally, we thank [3]'s EEG dataset laudable availability in the best spirit of reproducible science efforts.

## ACKNOWLEDGMENTS

P.L.C.R gratefully acknowledges the support from the CNPq 130765/2014-7 grant and L. A. B. to the CNPq 307163/2013-0 grant.

## REFERENCES

[1] M. Siegel, T. J. Buschman, and E. K. Miller, "Cortical information flow during flexible sensorimotor decisions," pp. 1–5.

[2] M. G. Preti, F. I. Karahanoglu, N. Leonardi, F. Grouiller, M. Genetti, M. Seeck, S. Vulliemoz, and D. V. D. Ville, "Functional Network Dynamics in Epilepsy Revealed By Dynamic Functional Connectivity and Eeg," p. 146318, 2014.

[3] G. Plomp, C. Quairiaux, C. M. Michel, and L. Astolfi, "The physiological plausibility of time-varying Granger-causal modeling: Normalization and weighting by spectral power," *NeuroImage*, vol. 97, pp. 206–216, 2014.

[4] M. Ding, S. L. Bressler, W. Yang, and H. Liang, "Short-window spectral analysis of cortical event-related potentials by adaptive multivariate autoregressive modeling: data preprocessing, model validation, and variability assessment," *Biological cybernetics*, vol. 83, no. 1, pp. 35–45, 2000.

[5] E. Moller, B. Schack, M. Arnold, and H. Witte, "Instantaneous multivariate EEG coherence analysis by means of adaptive high-dimensional autoregressive models," *Journal of neuroscience methods*, vol. 105, no. 2, pp. 143–158, 2001.

[6] L. A. Baccala and K. Sameshima, "Generalized partial directed coherence," in *Digital Signal Processing, 2007 15th International Conference on*. IEEE, 2007, pp. 163–166.

[7] P. L. C. Rodrigues and L. A. Baccalá, "A new algorithm for neural connectivity estimation of EEG event related potentials," in *International Conference of the IEEE Engineering in Medicine and Biology Society, EMBC'15*, no. 6, 2015, pp. 3787–3790.

[8] L. A. Baccala, C. S. N. de Brito, D. Y. Takahashi, and K. Sameshima, "Unified asymptotic theory for all partial directed coherence forms," *Philosophical Transactions of the Royal Society A: Mathematical, Physical and Engineering Sciences*, vol. 371, no. 1997, pp. 20 120 158–20 120 158, Jul. 2013.

[9] H. Akaike, "A new look at the statistical model identification," *IEE Transactions on Automatic Control*, vol. 19, pp. 716–723, 1974.

[10] D. Y. Takahashi, L. A. Baccalá, and K. Sameshima, "Connectivity inference between neural structures via partial directed coherence." *J. Appl. Stat.*, vol. 34, no. 10, pp. 1259–1273, 2007.

[11] F. H. Lopes da Silva, a. Hoeks, H. Smits, and L. H. Zetterberg, "Model of brain rhythmic activity - The alpha-rhythm of the thalamus," *Kybernetik*, vol. 15, no. 1, pp. 27–37, 1974.

[12] B. H. Jansen and V. G. Rit, "Electroencephalogram and visual evoked potential generation in a mathematical model of coupled cortical columns," *Biological cybernetics*, vol. 73, no. 4, pp. 357–366, 1995.

[13] O. David and K. J. Friston, "A neural mass model for MEG/EEG:," *NeuroImage*, vol. 20, no. 3, pp. 1743–1755, Nov. 2003.

[14] C. Quairiaux, P. Mégevand, J. Z. Kiss, and C. M. Michel, "Functional development of large-scale sensorimotor cortical networks in the brain." *The Journal of neuroscience : the official journal of the Society for Neuroscience*, vol. 31, no. 26, pp. 9574–9584, 2011.

[15] P. J. Durka, J. . Zygierewicz, H. Klekowicz, J. Ginter, and K. J. Blinowska, "On the Statistical Significance of Event-Related EEG Desynchronization and Synchronization in the Time-Frequency Plane," *IEEE TRANSACTIONS ON BIOMEDICAL ENGINEERING*, vol. 51, no. 7, 2004.

[16] A. Korzeniewska, C. M. Crainiceanu, R. Kuś, P. J. Franaszczuk, and N. E. Crone, "Dynamics of event-related causality in brain electrical activity," *Human Brain Mapping*, vol. 29, no. 10, pp. 1170–1192, 2008.

[17] L. A. Baccalá and K. Sameshima, "Partial directed coherence," in *Methods in Brain Connectivity Inference through Multivariate Time-Series Analysis*, K. Sameshima and L. A. Baccalá, Eds. CRC Press, 2014, pp. 57–73.

[18] R. G. Stockwell, L. Mansinha, and R. P. Lowe, "Localization of the complex spectrum: The S transform," *IEEE Transactions on Signal Processing*, vol. 44, no. 4, pp. 998–1001, 1996.